Single-neutron knockout reactions: Application to the spectroscopy of ^{16,17,19}C

V. Maddalena,[1,2] T. Aumann,[1,*] D. Bazin,[1] B. A. Brown,[1,2] J. A. Caggiano,[1,2,†] B. Davids,[1,2] T. Glasmacher,[1,2] P. G. Hansen,[1,2] R. W. Ibbotson,[1,‡] A. Navin,[1,§] B. V. Pritychenko,[1,2] H. Scheit,[1,2,‖] B. M. Sherrill,[1,2] M. Steiner,[1] J. A. Tostevin,[3] and J. Yurkon[1]

[1]*National Superconducting Cyclotron Laboratory, Michigan State University, East Lansing, Michigan 48824*

[2]*Department of Physics and Astronomy, Michigan State University, East Lansing, Michigan 48824*

[3]*Department of Physics, School of Physics and Chemistry, University of Surrey, Guildford, Surrey GU2 7XH, United Kingdom*

(Received 23 August 2000; published 24 January 2001)

The structure of the neutron-rich carbon isotopes ^{16,17,19}C has been investigated using one-neutron knockout reactions on a ^{9}Be target at approximately 60 MeV/nucleon. Partial cross sections and associated momentum distributions corresponding to final states of the ^{15,16,18}C residues were measured and compared with predictions based on a shell-model theory and an eikonal model of the reaction mechanism. Spectroscopic factors and l-value assignments are given. The ground-state spins of ^{17,19}C are $\frac{3}{2}^{+}$ and $\frac{1}{2}^{+}$, respectively. It is suggested that the accepted one-neutron separation energy for the ground state of ^{19}C needs to be revised upwards.

DOI: 10.1103/PhysRevC.63.024613 PACS number(s): 21.10.Jx, 25.60.Je, 27.20.+n

I. INTRODUCTION

Single-nucleon transfer reactions at low beam energies have been of great importance for understanding nuclear structure since they identify directly single-particle components of the nuclear wave function [1–3]. The classic tools have been stripping and pickup reactions, such as the (d,p) and (p,d) reactions, and the analogous reactions for probing proton states. For medium mass and heavy targets these light ions have a short mean free path inside the nucleus. The reactions are therefore surface dominated and probe the nuclear wave function in this region. They can be described as one-step processes involving the transfer of a nucleon to or from a given single-particle state. The development of theoretical methods such as the distorted-waves Born approximation (DWBA) has facilitated the use of transfer reactions to make angular momentum assignments from the shapes of angular distributions, and to deduce spectroscopic factors from the magnitudes of measured cross sections.

We have recently begun the development of a new technique suited for spectroscopic studies of rare nuclei produced with low intensity as beams from fragmentation reactions. The projectile residues formed by removing a single nucleon in the interaction with a light target are observed in inverse kinematics. The final states of the heavy residues are identified by their gamma decay [4–8]. The gamma rays tag reactions leading to individual discrete final levels and allow a determination of differential and integrated partial cross sections. It is possible to extend this technique to unbound final states by reconstructing the invariant mass (or other parameters of the intermediate state) from observations of the breakup products, see the recent work of Chen *et al.* [9] dealing with proton knockout from ^{11}Be leading to the unbound systems ^{10}Li and ^{9}He.

The recoil momentum of the heavy residue conveys information equivalent to the ''missing momentum'' obtained by reconstructing a reaction with light particles, e.g., the classical $(p,2p)$ knockout reactions. The shape of the longitudinal distribution identifies the orbital angular momentum l of the removed nucleon, while the absolute removal cross section determines the spectroscopic factors. The transverse momentum components carry essentially the same information, but they are more sensitive to contributions from the reaction mechanism such as Coulomb deflection and diffractive scattering.

The principal virtue of our technique for the spectroscopy of rare isotopes is its high sensitivity, which is of paramount importance in experiments aimed at exploring nuclei at the limits of particle stability, the so-called drip lines. This is illustrated in the following, where we present results from reactions with an incident beam intensity of less than one particle per second. The special experimental strength of the technique lies in the high energy of the beam particles and the detection of only the heavy residue. The high energy allows the use of thick targets and gives a strong forward focusing and hence a detection efficiency close to unity. It also allows the secondary beam and ''tertiary'' fragments to be tracked particle by particle, so that there is essentially no background. There are also important theoretical advantages. The high beam energies invite the use of reaction models, based on the sudden and the eikonal approximations [5,10], which have high predictive power. These methods can be used to relate the measured single-nucleon removal cross sections to theoretical spectroscopic information using, as in our previous work, a fixed set of theoretical input parameters.

The first applications of the knockout reaction method were aimed at clarifying specific features of exotic nuclei

*Present address: Gesellschaft für Schwerionenforschung, Planckstr. 1, 64291 Darmstadt, Germany.

†Present address: Physics Division, Argonne National Laboratory, Argonne, IL 60439.

‡Permanent address: Brookhaven National Laboratory, Upton, NY 11973-5000.

§Permanent address: Nuclear Physics Division, Bhabha Atomic Research Center, Trombay, Mumbai 400 085, India.

‖Present address: Max-Planck-Institut für Kernphysik, Postfach 10 39 80, D-69029 Heidelberg, Germany.

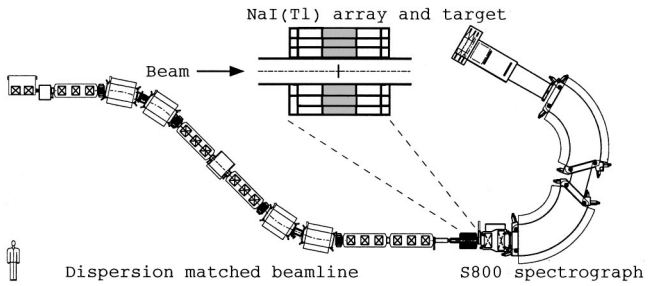

FIG. 1. Experimental setup. The dispersion-matched beam line delivers a secondary beam of radioactive ions on the target arrangement shown schematically in the inset. The target is surrounded by an array of 38 NaI(Tl) detectors, 20 cm long and 5 cm in diameter, which detect gamma rays in coincidence with projectilelike fragments measured in the S800 spectrograph.

that are otherwise well understood, such as the l assignments and spectroscopic factors for the presumed proton halo states of ^{26,27,28}P [4], and the spectroscopic factors linking known states in ^{10,11,12}Be [5,6,8], and in ^{13,14}B [7]. In this paper we present results for the neutron-rich carbon isotopes ^{16,17,19}C about which much less is known. However, they have been the subject of a number of recent theoretical and experimental studies [11–25]. We show, in particular (in agreement with Ref. [18]), that the ^{19}C ground state is similar to ^{11}Be and has a well-developed halo.

This paper begins with an outline of the essential features of the experimental and theoretical techniques used. Separate sections then present the results for each projectile, and detailed discussions of previous experimental and theoretical work are deferred to these parts of the paper. Finally, the conclusion offers some comments and a perspective on the potential of knockout reactions for precise single-particle structure studies with beams of rare isotopes.

II. EXPERIMENTAL TECHNIQUES

The experiments were performed at the National Superconducting Cyclotron Laboratory (NSCL) at Michigan State University. Radioactive beams of ^{16,17,19}C at approximately 60 MeV/nucleon were produced by fragmentation of an 80 MeV/nucleon ^{22}Ne primary beam on a thick ^{9}Be target. These secondary beams were purified in the A1200 fragment separator [26] by the combination of magnetic analysis and an intermediate degrader. The resulting beam was delivered to the experimental setup shown in Fig. 1, consisting of three parts: a dispersion-matching beam line, a target surrounded by an array of NaI(Tl) gamma detectors [27], and the S800 spectrograph [28] used for detecting the projectile residues from the reaction.

A. Cross section and momentum distribution of the knockout residue

The A1200 separator has been designed to accept a large momentum bite, up to 3% in normal operation. One technique for performing high resolution experiments with such beams is the use of a dispersion-matched system, in which the spread in incident momentum is compensated by dispersing the secondary beam on the reaction target and using the magnification of the spectrograph to cancel its dispersion. The S800 spectrograph [28] has been designed to operate in this way. Due to the large dispersion of the S800, the beam must be limited to a spread in relative momentum of 0.5%. In this case, it is possible to study reaction products at a relative momentum resolution of 0.025%. The spectrograph is characterized by a large angular acceptance (up to 20 msr solid angle, $\pm 5°$ horizontal, $\pm 3.5°$ vertical, dispersive direction) and by a momentum acceptance of $\pm 2.5\%$. The position and angles of the fragments were determined by two x/y position-sensitive cathode-readout drift chambers [29] at the focal plane of the spectrograph.

The incident ^{16,17,19}C projectiles were dispersion matched and struck a 228 mg/cm^2 ^{9}Be target. The average beam energies at the target mid-plane were 62 MeV/nucleon for ^{16,17}C and 57 MeV/nucleon for ^{19}C. The beam intensities were of 100–300 particles/s for ^{16,17}C and of as little as $\simeq 0.5-1$ particles/s for ^{19}C. Since the incident beams usually contain several products, the intensities of the projectiles of interest were measured in short exposures with the setting of the spectrograph adjusted to the full beam momenta. After this, long exposures at appropriately reduced field settings identified the ^{15,16,18}C residues. Their full momentum distributions were reconstructed with the ion optics code COSY INFINITY [30]. The intensities of the beams and residues were normalized using the signals from a beam-line timer, a scintillator placed at the end of the A1200 separator.

At the focal plane of the S800, a segmented ionization chamber and a 5 cm thick plastic scintillator measured the energy, energy loss, and time-of-flight of the residues. These data were used for particle identification purposes. The cross sections for one-neutron removal reactions were calculated as the yield of detected fragments divided by the yield of incident projectiles, taking into account the thickness and number density of the ^{9}Be target.

The spectrograph acceptance provided complete momentum distributions for the narrow distributions corresponding to low angular momentum ($l=0,1$) of the removed nucleon. The tails of higher l distributions were lost, due to both the angular and the momentum acceptance. Corrections for these losses were obtained with the following procedures. To estimate losses due to the geometrical acceptance, Monte Carlo simulations of the S800 response were performed. The angular acceptance corrections thus obtained were applied to the measured momentum distributions. Due to the finite momentum acceptance, the momentum distributions corresponding to $l=2$ needed careful examination, as only the contribution of the central part was measured. The additional contributions from the (unobserved) tails, typically a 10% correction, were estimated from the theoretical curves used to interpret the measured data and described in Sec. III B.

The measured cross sections, corrected for angular and acceptance losses, are listed in Table I and were used to extract the absolute partial cross sections, obtained from the gamma-ray data as described below. The total error of 12% in the cross sections obtained for one-neutron removal reactions from the ^{16,17}C projectiles includes uncertainties in target thickness, incident particle rate, particle identification,

TABLE I. Partial cross sections σ (in mb) and branching ratios b (in %) for the various final states I^π in the residues produced in ^{9}Be(^{16,17}C, ^{15,16}C)X at $E=62$ MeV/nucleon and in ^{9}Be(^{19}C, ^{18}C)X at $E=57$ MeV/nucleon. The theoretical cross sections σ_{th} are calculated from Eq. (1) using the WBP spectroscopic factors C^2S and the single-particle cross sections σ_{sp}. For ^{16}C the values of σ_{th} include overlap factors of 0.897 and 0.948, respectively (see text). The neutron separation energy of ^{19}C was assumed to be 0.8 MeV.

	E(MeV)	I^π	l	C^2S	σ_{sp}	σ_{th}	σ_{exp}	b_{th}	b_{exp}
(^{16}C, ^{15}C)	0.0	$\frac{1}{2}^+$	0	0.60	64	34	32±6	44	42±6
	0.74	$\frac{5}{2}^+$	2	1.23	37	43	45±7	56	58±6
σ_{tot}						77	77±9		
(^{17}C, ^{16}C)	0.0	0^+	2	0.03	53	2	22±11	2	19±9
	1.77	2^+	0	0.16	75	12	16±7	12	14±6
			2	1.44	37	53	44±11	53	38±8
			sum			65	60±12	65	52±8
	4.1 [a]	$2,3^{(+)},4^+$	0	0.22	50	11	2±2	11	2±2
			2	0.76	29	22	31±7	22	27±5
			sum			33	33±7	33	29±5
σ_{tot}						100	115±14		
(^{19}C, ^{18}C)	0.0	0^+	0	0.58	136	79	148±50	46	56±9
	1.6 [b]	2^+	2	0.48	34	16			
	4.0 [b]	0^+	0	0.32	45	14			
	4.9 [b]	$2^+,3^+$	2	2.44	26	63			
			sum			93	116±45	54	44±11
σ_{tot}						172	264±80		

[a]The components of this group have been analyzed together. We identify them with three states predicted by theory in the range 4.9–5.7 MeV. The main contributions were given by at least two components.
[b]All excited states in ^{18}C were analyzed as one group (see text). The energy 1.6 MeV for the 2^+ is the experimental value; the WBP calculation gives 2.16 MeV.

and acceptance. For the ^{19}C projectile a total error of 30% was estimated, due to significant fluctuations in the rate of incident projectiles.

As is pointed out in Secs. I and III, the momentum components parallel to the beam direction are those that carry a clean signature of the momentum content related to the single-particle state in question. We show the results in the laboratory system, and the measured quantity is actually the total momentum, which has been projected onto the beam axis to give the quantity $P_{||}$ used in the figures of the present paper. Since the residue's deflection angle is small, typically a few degrees, the difference between the total momentum and the parallel momentum is small. The laboratory distributions are broadened by the relativistic γ factor, which has to be included in the comparisons with theory.

B. Gamma-ray detection

The excited states of the residues were tagged by an inner ring of 11 cylindrical NaI(Tl) scintillators surrounding the target. Each scintillator was read out by two photomultiplier tubes, one at each end, thus allowing the determination of both the energy and the interaction point of the photon in the detector. The position information provided by the array made it possible to correct for the Doppler shift in the energy of the γ rays emitted by the fast ($\beta \simeq 0.34$) residues. The back transformation to the center-of-mass (c.m.) system, however, does not generate the spectrum that would have been observed from a source at rest due to the energy dependence of the detection efficiency and, especially, events in which radiation has escaped from the crystal. Examples of these are annihilation radiation and Compton-scattered photons. Since the reconstruction cannot identify these features, the part of the response function that lies below the full-energy peak gets smeared. This may seem unimportant since the full-energy peaks obviously are reconstructed correctly. However, an accurate understanding of the measured envelope of the gamma spectrum requires knowledge also of the shape of the continuum distributions underlying the peaks. For the decomposition of the measured spectrum, complete response functions were constructed in a numerical simulation in the following way.

For a gamma ray of a given energy, assumed to be isotropically emitted in the projectile c.m. system, a sequence of Lorentz-boosted γ events with the appropriate angular distribution was generated in a Monte Carlo procedure. These were subsequently used in the Monte Carlo code GEANT [31], which simulated the energy deposited in the detectors as well as losses generated by interactions with chamber walls and detector mounts. One million events were generated for a given energy. For each event the (random) outcome was randomly broadened by the energy resolution, which was assumed to scale with the square root of the energy and was fixed to the measured resolution corresponding to a full width at half maximum (FWHM) of 7.5% at 1.33 MeV.

Based on the spatial resolution of 1.5 cm FWHM, the sequence of simulated γ signals were corrected event-by-event for the Doppler shift to construct the apparent energy in the c.m. system. Histograms of the simulated events created the reference line shapes. The resulting shapes were approximated by smooth analytical curves (to eliminate statistical fluctuations from the Monte Carlo procedure) and were used for fitting the observed spectra. The reliability of the simulations was verified by comparing measured and simulated γ-ray spectra from (necessarily stationary) calibration sources. An agreement to within 10% in the absolute intensity was found.

A complication in the data analysis was the presence of a continuum distribution varying approximately exponentially with energy. We attribute this to neutrons, gamma rays, and charged particles produced in the target and to their secondary interactions with construction materials and the scintillator. This distribution has been seen consistently in previous experiments [4,6–8] with an intensity, for gamma energies above 0.25 MeV, of approximately 9% per outgoing fragment. Although it reduces the sensitivity to weak transitions (the ^{17}C analysis shows an example of this), it does not significantly interfere with the fitting of the gamma-ray energies and intensities.

The measured branching ratios deduced from the gamma intensities (with indirect feeding taken into account) are given in Table I. In the case of the reaction of ^{17}C leading to the first excited level of ^{16}C the momentum distributions of the residues observed in coincidence with gamma rays corresponded to a mixture of the l values 0 and 2. This has served to subdivide the experimental branching ratio further, corresponding to the two l values. A similar case was found in ^{14}B [7].

III. THEORETICAL ANALYSIS

The application of knockout reactions for spectroscopic studies grew out of studies of the neutron halo [32], where the large cross sections and narrow momentum distributions observed in the breakup of neutron halo systems provided evidence for the large size of the halo. It was shown by Bertsch *et al.* and others [33,34,10] that the eikonal approximation, previously used for nucleon-nucleus scattering at high energies, gave a good description of the cross sections for such reactions on light targets. From this also follows that the outgoing fragment's longitudinal momentum distribution reflects the momentum content of the wave function in the volume sampled by the projectile's interaction with the target [35–37]. The cross sections and momentum distributions are very sensitive to the angular momentum and separation energy of the nucleon in the initial state.

More recently it has been shown that there are also appreciable cross sections for the removal of a nucleon from the occupied nonhalo single-particle states in the projectile. An example of this is furnished by the example of the light phosphorus isotopes, where the knockout of the halo proton from the ground state constitutes only 30–55 % of the total measured knockout cross section [4]. Even for the very pronounced single-neutron halo nucleus ^{11}Be, one finds by comparing the original inclusive experiment [38] on the ^{9}Be(^{11}Be,^{10}Be)X reaction at 66 MeV/nucleon with the exclusive measurement with gamma rays in coincidence [6], that 22% of the cross section populates excited levels of the ^{10}Be residues. The momentum distributions of the heavy residues arising from knockout from deeply bound states can be calculated using the same techniques as for the halo states.

Similarly, extending the eikonal approximation as applied to halo nucleus ground states to treat the removal of a nonhalo nucleon from the initial state, Tostevin [5] writes the cross section $\sigma_{\rm th}(I^\pi)$, for populating a given final state I^π of the residue or core, as

$$\sigma_{\rm th}(I^\pi)=\sum_j C^2S(I^\pi,nlj)\sigma_{\rm sp}(S_n,nlj). \qquad (1)$$

Here C^2S, the spectroscopic factor for removal of a nucleon with given single-particle quantum numbers (nlj), expresses the parentage of this configuration in the initial state with respect to the specific state I^π of the remaining nucleons. Following nucleon removal this is assumed to be the final state of the residue, which is therefore assumed to behave as a spectator particle and to interact at most elastically with the target [39]. The sum in Eq. (1) is taken over all configurations which have a nonvanishing parentage. The $\sigma_{\rm sp}$ are the single-particle removal cross sections, which are strongly dependent on the orbital angular momentum l and the neutron separation energy S_n. We discuss the calculation of these quantities below.

The approach of the present paper and its predecessors has been adopted in recent work by Sauvan *et al.* [24], who have measured inclusive one-neutron removal cross sections and momentum distributions for 23 nuclei in the $p-sd$ shell. The results are in good agreement with calculations based on techniques that are essentially identical to those used here. In particular, the results for the inclusive absolute cross sections suggest that the method may actually be more accurate than the $\pm 20\%$ conservative estimate proposed in the following. It is also interesting to compare this and our results with the measurements of charge-changing cross sections ($\sigma_{\rm cc}$) reported by Chulkov *et al.* [21]. In their analysis they obtain total neutron-removal cross sections σ_{-xn} by taking the difference between interaction cross sections σ_I and $\sigma_{\rm cc}$. While the σ_I and $\sigma_{\rm cc}$ can be discussed in terms of global density distributions, Chulkov *et al.* find that the σ_{-xn} show a more complicated behavior suggesting the influence of nuclear structure effects. The present work shows how these can be accounted for in the one-neutron removal channel through the use of spectroscopic factors calculated from a many-particle wave function. An example of how these effects can show up in the two-neutron removal channel is offered by our recent experiment on ^{12}Be [8], where a sizable fraction of the one-neutron removal cross section populates the unbound $0d_{5/2}$ state in ^{11}Be.

TABLE II. The reaction ^{9}Be(^{17}C,^{16}C)X at $E=62$ MeV/nucleon, for a ^{17}C ground-state spin $J^{\pi}=\frac{5}{2}^{+}$ or $\frac{1}{2}^{+}$, see Table I.

$J^{\pi}(^{17}\mathrm{C})$	E(MeV)	I^{π}	l	C^2S	σ_{sp}	σ_{th}	σ_{exp}	b_{th}(%)	b_{exp}(%)
$\frac{5}{2}^{+}$	0.0	0^{+}	2	0.70	53	37	22 ± 11	35	19 ± 9
	1.77	2^{+}	0	0.10	75	8	16 ± 7	7	14 ± 6
			2	0.22	37	8	44 ± 11	7	38 ± 8
			sum			16	60 ± 12	14	52 ± 8
	4.1 [a]	$2,3^{(+)},4^{+}$	0	0.39	50	20	2 ± 2	19	2 ± 2
			2	1.16	29	34	31 ± 7	32	27 ± 5
			sum			54	33 ± 7	51	29 ± 5
σ_{tot}						107	115 ± 14		
$\frac{1}{2}^{+}$	0.0	0^{+}	0	0.64	148	95	22 ± 11	57	19 ± 9
	1.77	2^{+}	2	0.39	37	14	60 ± 12	9	52 ± 8
	3.03	0^{+}	0	0.29	59	17	–	10	–
	4.1 [a]	$2,3^{(+)}$	2	1.39	29	40	33 ± 7	24	29 ± 5
σ_{tot}						166	115 ± 14		

[a]The components of this group have been analyzed together. We identify them with three states predicted by theory in the range 4.9–5.7 MeV. The main contributions were given by at least two components.

A. Theory of the spectroscopic factors of the neutron-rich carbon isotopes

A number of recent papers cited above have discussed the properties of the heavy carbon isotopes within the framework of particle-core-coupling models, cluster models and global density distributions. Although such models provide qualitative insight into the structure and resulting cross sections of the ground states, they do not furnish a unified description of all states. We have instead relied on shell-model calculations. The natural shell-model space for these nuclei is the complete set of basis states spanned by the neutrons in $1s_{1/2}$, $0d_{5/2}$, and $0d_{3/2}$ (sd-shell) orbits together with protons in $0p_{3/2}$ and $0p_{1/2}$ (p-shell) orbits.

The Hamiltonian for the neutrons in the sd-shell is well established by Wildenthal's USD interaction [40]. The USD two-body matrix elements are assumed to scale with mass as $(18/A)^{0.3}$, which is about the form expected for a finite range interaction [40]. However, there may be structure and/or binding-energy considerations which would cause a deviation from this dependence; the comparisons we make in this work will serve as a test of this assumption. The p-shell Hamiltonian is also well established [41]. The proton-neutron ($p-sd$) part of the Hamiltonian is based upon the work of Warburton and Brown (WB) [41]. WB considered all of the known data (165 levels) in the mass region $A=10-20$ which could be associated with the $p-sd$ Hamiltonian. Among the 165 energy-level data considered were those of ^{15}C: $\frac{1}{2}^{+}$ and $\frac{5}{2}^{+}$; ^{16}C: 0^{+}, 2^{+}, 3^{+}, and 4^{+}; ^{17}C: $\frac{3}{2}^{+}$; ^{18}C: 0^{+} and 2^{+}; and ^{19}C: $\frac{1}{2}^{+}$.

Two types of p-sd Hamiltonians were developed: (1) WBT was modeled on a set of two-body matrix elements (TBME) obtained from a bare G matrix, and (2) WBP was modeled on a one-boson exchange potential (OBEP) which includes the one-pion exchange potential (OPEP) (fixed at its known strength) and a long-range (monopole) interaction. For input to the shell-model calculations, WBP and WBT are expressed in terms of TBME. Both mass-dependent and mass-independent TBME were studied, and the latter gave the best agreement with the 165 energy data. For WBT, 28 linear combinations of the 95 p-sd TBME were adjusted to fit the data. For WBP, 10 parameters associated with the strength of the OBEP terms were varied. The root-mean-squared (rms) deviations for the 165 p-sd data were 389 keV for WBP and 330 keV for WBT. Comparisons between the predictions made with WBP and WBT will give an indication of the theoretical error in these type of calculations. WBP is an evolution of the Millener-Kurath potential model for the p-sd interaction which was developed earlier [42].

The WBP and WBT interactions have been used to predict many properties of nuclei in the $A=10-20$ mass region [43,6,8]. In general, the wave functions and spectroscopic properties with WBP and WBT are similar, but there are differences in the energy-level details, especially when the levels are spaced more closely than the 350 keV rms deviation established in their derivation. In the present context, the calculations provide both level energies and the required spectroscopic factors C^2S. These are presented in Tables I and II and discussed in detail in the following sections.

For both ^{17}C and ^{19}C there is a triplet of low-lying levels with spin-parity $\frac{1}{2}^{+}$, $\frac{3}{2}^{+}$, and $\frac{5}{2}^{+}$. The ordering of these levels differs between WBP and WBT. WBP gives for ^{17}C: $\frac{3}{2}^{+}$ (ground state), $\frac{5}{2}^{+}$ at 0.03 MeV, and $\frac{1}{2}^{+}$ at 0.30 MeV; and for ^{19}C: $\frac{1}{2}^{+}$ (ground state), $\frac{5}{2}^{+}$ at 0.19 MeV, and $\frac{3}{2}^{+}$ at 0.62 MeV. WBT gives for ^{17}C: $\frac{5}{2}^{+}$ (ground state), $\frac{3}{2}^{+}$ at 0.08 MeV, and $\frac{1}{2}^{+}$ at 0.27 MeV; and for ^{19}C: $\frac{5}{2}^{+}$ (ground state), $\frac{1}{2}^{+}$ at 0.5 MeV, and $\frac{3}{2}^{+}$ at 0.40 MeV. The present experimental results give $\frac{3}{2}^{+}$ for the ^{17}C ground state and $\frac{1}{2}^{+}$ for the ^{19}C ground state. Thus the WBP interaction is favored in this respect. However, it does not rule out WBT since the required levels associated with the experimental spins are within the nominal 350 keV deviation expected. Details about the wave functions will be discussed in Sec. IV. The WBP interaction will be used for the spectroscopic factors. Generally, the spectroscopic factors obtained for WBP and

WBT are very similar, and we will comment on any important differences. The spectroscopic factors between the low-lying positive parity states are related to pickup from *s* and *d* orbitals. Pickup from the *p* orbitals leads to negative parity states at excitation energies above the neutron-decay threshold, and are thus not observed in the present experiment.

B. Theory of the single-particle cross sections

The cross sections $\sigma_{\rm sp}$ in Eq. (1) were calculated in the eikonal model [5]. The same input parameter set was used as in the reported analyses of Refs. [4,6–8]. The calculation of each single-particle cross section assumes that the removed nucleon is described by a normalized single-particle wave function with quantum numbers (nlj) moving with respect to the core of remaining nucleons in state $c \equiv I^{\pi}$. Such configurations are written $|\phi^c_{JM}\rangle$, where J is the magnitude and M the projection of the projectile's ground-state total angular momentum, $\mathbf{J}=\mathbf{I}+\mathbf{j}$.

Since only the residue is detected, and not the neutrons, these single-particle cross sections are a sum of the contributions from removal of the neutron due to elastic breakup (diffraction dissociation) and absorption (stripping) [39], $\sigma_{\rm sp}=\sigma^{\rm diff}_{\rm sp}+\sigma^{\rm str}_{\rm sp}$. These two contributions are computed separately, as integrals over the projectile's center of mass impact parameter, using [5]

$$\sigma^{\rm diff}_{\rm sp}=\frac{1}{2J+1}\int d\mathbf{b}\left[\sum_M \langle\phi^c_{JM}||(1-\mathcal{S}_c\mathcal{S}_n)|^2|\phi^c_{JM}\rangle - \sum_{M,M'}|\langle\phi^c_{JM'}|(1-\mathcal{S}_c\mathcal{S}_n)|\phi^c_{JM}\rangle|^2\right] \quad (2)$$

and

$$\sigma^{\rm str}_{\rm sp}=\frac{1}{2J+1}\int d\mathbf{b}\sum_M \langle\phi^c_{JM}|(1-|\mathcal{S}_n|^2)|\mathcal{S}_c|^2|\phi^c_{JM}\rangle. \quad (3)$$

Here the quantities $\mathcal{S}_c$ and $\mathcal{S}_n$ are the elastic *S* matrices, or profile functions [44,45], for the core-target and removed neutron-target systems, expressed as functions of their individual impact parameters. These are calculated using the optical limit of Glauber theory [46]. The neutron-core relative motion wave functions $|\phi^c_{JM}\rangle$ are calculated in a Woods-Saxon potential with radius and diffuseness parameters 1.25 and 0.7 fm. The depth of the potential was adjusted to reproduce the separation energy of the nucleon in the (initial) state with given nlj. In those cases where a more strongly bound nucleon is removed from a system which also binds a weakly bound and delocalized neutron, this few-body composite structure of the residue upon $\mathcal{S}_c$ was taken into account explicitly, as in Ref. [5].

Equation (3) allows a simple interpretation. It is the integral over impact parameter, and average over *M* substates, of the joint probability of the core being left intact by the reaction (given by the quantity $|\mathcal{S}_c|^2$) and of the neutron being absorbed [given by the quantity $(1-|\mathcal{S}_n|^2)$]. The diffractive cross section, Eq. (2), is derived within the spectator core plus nucleon model by using closure to eliminate the necessary integral over all continuum final states of the dissociated core and nucleon. The second term in Eq. (2) arises because we assume that the dominant bound states contribution from this closure relation is due to the bound state ϕ^c_{JM} of the core-nucleon effective Hamiltonian which has maximum overlap with the initial state. Contributions from any other bound states supported by the core-nucleon Hamiltonian take the form of inelastic amplitudes, are small, but will add terms to Eq. (2) which would reduce the calculated diffractive cross section. For halo states, Eqs. (2) and (3) make roughly equal contributions to the single-particle cross section. For more strongly bound states the contribution from Eq. (2) is typically a factor of 2–3 smaller than that of Eq. (3) and may be smaller. It will be interesting to test this assumption experimentally.

The essential parameters in the calculation of the functions $\mathcal{S}$ are an effective nucleon-nucleon interaction and the rms matter radii of the assumed Gaussian matter distributions for the core and target nuclei. The ^{9}Be matter radius was taken as 2.36 fm. The effective interaction, also assumed a Gaussian, used the free nucleon–nucleon cross sections [47] and the real-to-imaginary ratio for the forward scattering amplitude tabulated by Ray [48] for 100 MeV nucleons. The interaction range, of 0.5 fm, was chosen [5] so that the calculated reaction cross sections are consistent with measured values. Specifically, calculated reaction cross sections for the ^{12}C-^{12}C and ^{27}Al-^{12}C systems at 83 MeV/nucleon [49], and for the proton-^{9}Be system at 60 MeV/nucleon [50], were consistent with experiment.

The point-particle rms matter radii for the carbon isotopes were first reported in Refs. [51,52]; we use here the results of the recent paper by Ozawa *et al.* [17]. Our results are not very sensitive to the matter radius; for ^{19}C an overall increase of 10% reduces the calculated cross sections for removal of the halo or of more bound neutrons by 8% and 16%, respectively. The calculated single-particle cross sections, defined as the sum of the stripping and diffraction dissociation contributions, are given in Table I. The use of alternative microscopic descriptions of the neutron-target interaction, and corresponding $\mathcal{S}_n$, has been shown to calculate very similar $\sigma_{\rm sp}$ [53].

Theoretical calculations of the longitudinal momentum distributions of the core fragments were made in a simpler model, based on a black-disc approximation. In this, $\mathcal{S}_c$ and $\mathcal{S}_n$ are assumed to be unity outside of a cutoff impact parameter and zero inside [36]. These impact parameter cutoffs were chosen to reproduce core-target reaction cross section systematics [49] and the neutron-target reaction cross section of 306 mb at 60 MeV/nucleon. (The corresponding values are 286 and 298 mb when calculated for 62 and 57 MeV, respectively, with the parameters used for the partial cross sections. The widths of the momentum distributions are insensitive to the precise choice of target radius.) The neutron relative motion wave functions were calculated in a Woods-Saxon potential, as above. In this model the profile functions affect the limits of impact parameter integrations, and the momentum distribution takes the form of a one-dimensional Wigner transform of the wave packet produced in the reaction [36]. The integrated cross sections obtained with this

procedure agree well with those calculated using the more realistic profile functions. Test calculations show that the shapes of the momentum distributions are much less sensitive to the choice of the impact-parameter cutoff than are the absolute values of the cross sections. In the following, we present these calculated shapes scaled to fit the observed intensity, the idea being that the shape, taken separately, is the quantity that carries information on the l assignment. The absolute value of the partial cross section then leads to the spectroscopic factor.

An alternative treatment, by Bonaccorso and Brink, has also been applied to the longitudinal momentum distributions of neutrons from the breakup of halo states [54–56]. They use a semiclassical (constant velocity, straight line) approximation for the relative motion of the core and target, with a lower impact parameter cutoff, but a (nonsudden) quantum-mechanical treatment of the interaction of the neutron with the target. The treatment, which deals with the diffractive and the stripping parts in a consistent way, gives an excellent description of the angular distribution of neutrons following the breakup of ^{11}Be [54]. The breakup contribution to the heavy residue longitudinal momentum distributions discussed in the present paper can be inferred from that of the neutron in the rest frame of the projectile. For (^{11}Be, ^{10}Be$_{gs}$) breakup it was found [6] that the resulting shapes are essentially indistinguishable from those of the eikonal calculation. A recent application to the carbon isotopes [56] reported cross sections somewhat larger than those given in Table I, however, depending on the chosen set of optical parameters for the $n+^9$Be system, the agreement is better. Bonaccorso finds [57] for the case of ^{19}C at 60 MeV/nucleon and an assumed neutron separation energy of 0.5 MeV single-particle cross sections, given as (stripping, diffraction in mb), of (100, 76) in agreement with our (99, 71) for the ground state. For an assumed $l=2$ cross section to a 1.62 MeV excited level, she finds (21, 11) as compared with our values of (25, 11). Reference [56] reports an interesting feature arising from the inclusion of the spin dependence of the neutron interaction in the analysis. It turns out that different momentum signatures arise from the breakup of the $0d_{5/2}$ and $0d_{3/2}$ spin-orbit partners. The present data are not good enough to reveal this effect, but this prediction should certainly be kept in mind and investigated in future experiments.

IV. RESULTS AND DISCUSSION

A. The projectile ^{16}C

1. Previous theoretical and experimental work

The structure of the low-lying levels in ^{16}C has been investigated [58–61] in the reactions ^{14}C$(t,p)^{16}$C and ^{14}C$(t,p\gamma)^{16}$C. Tilley *et al.* [62] discuss properties and the level scheme, to which we return in Sec. IV B. The structure of ^{16}C is expected to correspond to ^{14}C$\otimes^{18}$O. Since ^{14}C is a near-magic nucleus, the simplest conjecture is that the neutron pair of ^{16}C should be similar to that of ^{18}O, which has a relatively pure s^2+d^2 two-particle configuration with spectroscopic factors [63] $C^2S(1s_{1/2})=0.38$ and $C^2S(0d_{5/2})=1.44$, and where the missing part is a $4p$-$2h$ collective contribution. The wave functions in Ref. [63] were later used in the study of the mirror nucleus ^{18}Ne [64] and successfully reproduced the observed Coulomb energy shifts. When the LSF model [63] is applied to ^{16}C, the s^2 and d^2 components are about equal and the spectroscopic factors would be about $C^2S(1s_{1/2})=0.93$ and $C^2S(0d_{5/2})=1.07$ [65]. As discussed in the next section, the origin of the difference between the ^{18}O and ^{16}C spectroscopic factors is mainly in the change in single-particle energies.

The experimental situation for the next lighter $N=10$ isotone ^{14}Be is interesting but less clear experimentally. The breakup reaction to ^{12}Be [66] leads to a narrow momentum distribution indicating a halo structure, presumably arising from a substantial s^2 component. The same is suggested by the beta-delayed neutron decay of ^{14}Be, which shows [67,68] an almost superallowed branch ($\log ft\approx 3.7$) to a 1^+ state (not directly observed) at 1–2 MeV excitation energy. The theory of the ^{14}Be beta decay has been discussed by Timofeyuk and Descouvemont [69]. A recent $2n$ pairing model calculation [70] suggests, somewhat surprisingly, a negative-parity ground state of ^{13}Be and spectroscopic factors of 0.9, 0.6, and 0.5 for single-neutron breakup to the $\frac{1}{2}^-$ ground state, the $\frac{1}{2}^+$ and $\frac{5}{2}^+$ s and d states, respectively.

2. Present shell-model results

For ^{18}O, WBP and WBT are equivalent to the sd–shell USD results with $C^2S(1s_{1/2})=0.30$ and $C^2S(0d_{5/2})=1.58$ [with the remaining in $C^2S(0d_{3/2})=0.12$ leading to a state at high excitation energy]. For ^{16}C, WBP gives $C^2S(1s_{1/2})=0.60$ and $C^2S(0d_{5/2})=1.23$, and WBT gives $C^2S(1s_{1/2})=0.78$ and $C^2S(0d_{5/2})=1.07$. One reason for the difference can be related to the ^{15}C spectrum with the $\frac{5}{2}^+$ excited state at 0.38 MeV with WBP and at 0.66 MeV with WBT, compared to the experimental energy at 0.74 MeV; and on this basis the WBT results are preferred. The spectroscopic factors depend upon the spacing of the single-particle energies and, in particular, the crossing of the single-particle energies between ^{17}O (where the $\frac{1}{2}^+$ is 0.87 MeV above the $\frac{5}{2}^+$) and ^{15}C, which gives rise to the large change between ^{18}O and ^{16}C.

3. Experimental results and discussion

The neutron knockout reaction on ^{16}C (neutron separation energy $S_n=4.25$ MeV [71]) leads to the two (only) bound levels of ^{15}C, the $\frac{1}{2}^+$ ground state and the $\frac{5}{2}^+$ state at 0.740 MeV [72]. The latter has a long half-life (2.60 ± 0.07 ns), which combined with the high velocity of the residues causes the γ rays to be emitted at a mean distance of 34 cm from the center of the detectors, which are only 20 cm long. This means that the Doppler correction scheme described in Sec. II B fails. In fact, most gamma rays are emitted outside of the apparatus reducing the detected intensity. Figure 2 shows the γ-ray spectrum measured in coincidence with ^{15}C residues without the Doppler back-correction.

Fortunately, accurate estimates of the continuum distribution are available from our previous experiments on ^{11}Be [6] and ^{12}Be [8]. In the latter case, the only γ has an energy of 0.320 MeV and provides, after normalization to the same

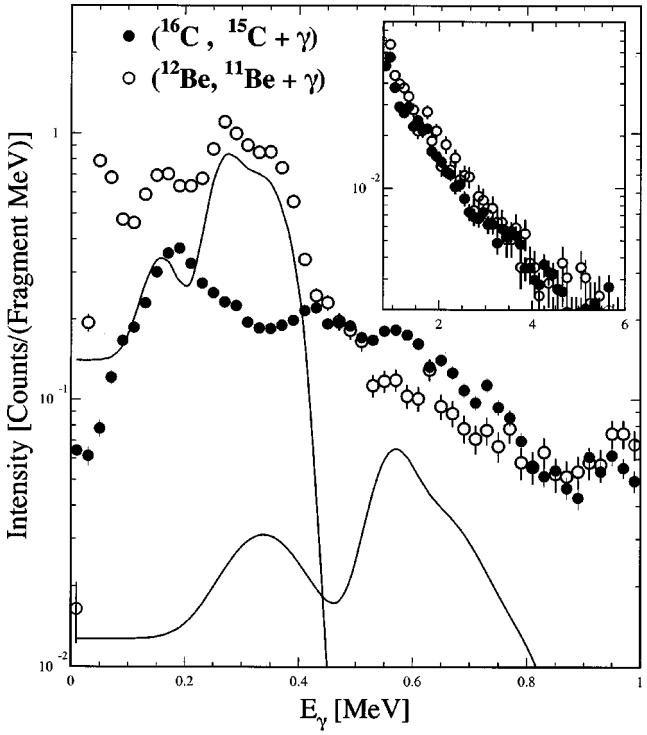

FIG. 2. Laboratory system γ-ray spectra from ^{9}Be(^{16}C,^{15}C $+\gamma$)X (filled circles) and ^{9}Be(^{12}Be,^{11}Be$+\gamma$)X (open circles), normalized to the number of projectile fragments. The solid lines are simulated response functions for the 0.74 MeV γ ray from the decay in flight of ^{15}C* and for the 0.32 MeV γ ray from ^{11}Be*. The inset shows experimental γ-ray spectra from ^{11}Be and ^{15}C for $E_\gamma > 1$ MeV. The ''tails'' above the γ lines, the only discrete lines present, are the continuum distributions discussed in the text.

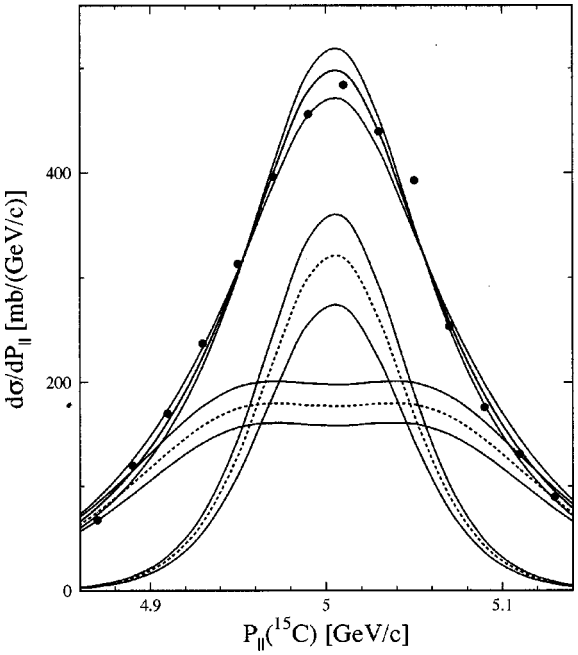

FIG. 3. Inclusive longitudinal momentum distribution of the ^{15}C fragments produced in one-neutron removal reactions of ^{16}C on a ^{9}Be target. The experimental errors are smaller than the size of the points. The full-drawn line is a fit with the short-dashed lines showing the individual theoretical components. The thin lines indicate the error limits allowed by the fit. The broad component corresponds to $58\pm6\%$ *d* wave and the narrow one to $42\mp6\%$ *s* wave.

number of outgoing residues, an excellent estimate of the continuum distribution in the 0.740 MeV region. (The more indirect estimate of [6] agrees well with the ^{16}C and ^{12}Be results.) Above this, the two agree in shape and intensity to within 15%. The ^{16}C data in Fig. 2 show a clear excess above the ^{12}Be background in the region 0.5–0.8 MeV. A simulated response curve of the NaI array to the isomeric decay was generated in a Monte Carlo procedure in which the gamma events were assumed to appear downstream along the beam axis with the appropriate exponential distribution. The response was then simulated by the GEANT code, as before. The resulting efficiency turned out to be reduced by a factor of 4 as compared to instantaneous emission. A combined fit to the components in Fig. 2 gave an absolute branch of $30\pm10\%$ to the excited $\frac{5}{2}^+$ state with the error determined by the statistics alone. However, this result is almost certainly an underestimate, corresponding to an overestimate of the detection efficiency. This is because the simulation did not include the size and divergence of the incoming beam and the angular spread of the outgoing residues, nor did it include the way that these affect the absorption of the low-energy gamma rays emitted in the backward direction. We take this analysis as providing a semiquantitative but direct indication of the contribution of the appearance of the d^2 component in the ^{16}C ground state. The statistics in Fig. 2 are insufficient to permit an extraction of the momentum distribution to the excited level, but since the assignments in the ^{15}C nucleus are well established, this is probably of little importance.

A more accurate estimate of the branching ratio was obtained from the measured inclusive longitudinal momentum distribution of the residues shown in Fig. 3. Experience from previous experiments has shown that the theoretically calculated momentum distributions lead to shapes that are well reproduced by experiment. As these, furthermore, are very different for *s*- and *d*-state knockout, it is easy to arrive at the overall fit (envelope) shown in the figure. The criterion adopted to fix the limits of the fit was to consider the momentum acceptance range of $\pm2.5\%$. The geometrical loss for the inclusive spectrum was estimated to be 2% by the method described in Sec. II A. The extrapolation of the envelope gave momentum acceptance losses of 4%. Both corrections were applied to the measurement to give the total (inclusive) cross section of 77 ± 9 mb reported in Table I. This agrees reasonably well with the inclusive one-neutron removal cross section of 65 ± 6 mb for ^{16}C recently measured at 55 MeV/nucleon by Sauvan *et al.* [24] and their calculated value of 75 mb is essentially identical with ours. The resulting intensity of the broad (*d*-wave) component gave $58\pm6\%$ excited state contribution to the cross section. This is twice the value obtained from the analysis of coincident gamma rays and suggests that the simulation of the delayed events overestimated the γ detection efficiency.

Table I compares the measured partial cross sections with the theoretical results obtained as the product of the spectro-

scopic factor and the single-particle cross section as discussed in Sec. III. For the case of ^{16}C, it was also necessary, as in Ref. [8], to take into account the radial mismatch factor arising from the difference in single-particle potential between the two nuclei. This is not included in the shell-model calculations used here. The effective neutron separation energies (to which the wave function must be adjusted) are for ^{15,16}C, respectively, 1.22 and 4.25 MeV for the *s* state and 0.48 and 4.99 MeV for the *d* state. In the table the correction has been included in the theoretical partial cross sections with the values 0.897 and 0.948. We see that the nonoverlap effect is less important for the $l=2$ state, which is already spatially constrained by the angular momentum barrier. For the direct comparison with the shell-model occupancies of the ^{16}C neutron pair, we divide the experimental cross sections by the corresponding single-particle cross sections and mismatch factors and obtain spectroscopic factors $C^2S^*_{\rm exp}$ corresponding to the quantities defined in [8]. The resulting values and experimental error limits are 0.56 ± 0.10 ($\frac{1}{2}^+$) and 1.28 ± 0.20 ($\frac{5}{2}^+$). They are in excellent agreement with the theoretical spectroscopic factors 0.60 and 1.23, respectively.

B. The projectile ^{17}C

1. Previous theoretical and experimental work

The levels of ^{17}C have been studied in the multinucleon transfer reaction ^{48}Ca(^{18}O,^{17}C)^{49}Ti by Fifield *et al.* [73]. The lowest state, interpreted as the ground state, has a neutron separation energy of 0.729 ± 0.018 MeV [71] based on this and a previous measurement. Fifield *et al.* found a cross section five times larger to a level at 0.395 MeV. The analysis by Warburton and Millener [74] interprets this as the $\frac{5}{2}^+$ state, expected to be favored in a two-step transfer reaction; see, for example Ref. [75]. Their analysis of the beta decay data for ^{17}N [76,77] supports this conclusion and allows the $\frac{5}{2}^+$ ground-state assignment to be ''eliminated model independently.'' Of the remaining likely spin-parity assignments for the ground state, $\frac{1}{2}^+$ and $\frac{3}{2}^+$, they prefer the latter, but both remain ''quite possible.'' Several theoretical papers [19,22,23] have dealt with the one-neutron removal reactions on ^{17}C.

2. Present shell-model results

As discussed in Sec. III A, the WBP and WBT interactions both present a triplet of low-lying states for ^{17}C. The present experimental results are in agreement only with the spectroscopic factors based upon the $\frac{3}{2}^+$ ground state. The WBP interaction gives a $\frac{3}{2}^+$ ground state and this will be used for further comparisons. However, for the given spin parity of $\frac{3}{2}^+$ the spectroscopic factors are very similar between WBP and WBT.

The $\frac{3}{2}^+$ state is a deformed component of the $(0d_{5/2},1s_{1/2})^3$ configuration. It is related to the $\Omega=\frac{3}{2}^+$ Nilsson orbital, but is also influenced by the low-lying nature of the seniority-three $\frac{3}{2}^+$ component of the $(d_{5/2})^3$ configuration for the three neutrons. A similar situation occurs for ^{21}Ne which has a $\frac{3}{2}^+$ ground state in agreement with the USD interaction [40]. The *sd*-shell USD value for the ^{21}Ne to ^{20}Ne spectroscopic factor is $C^2S(0d_{3/2})=0.028$ compared with the experimental upper limit of 0.03 [78]. This indicates that the $0d_{3/2}$ single-particle component is very small.

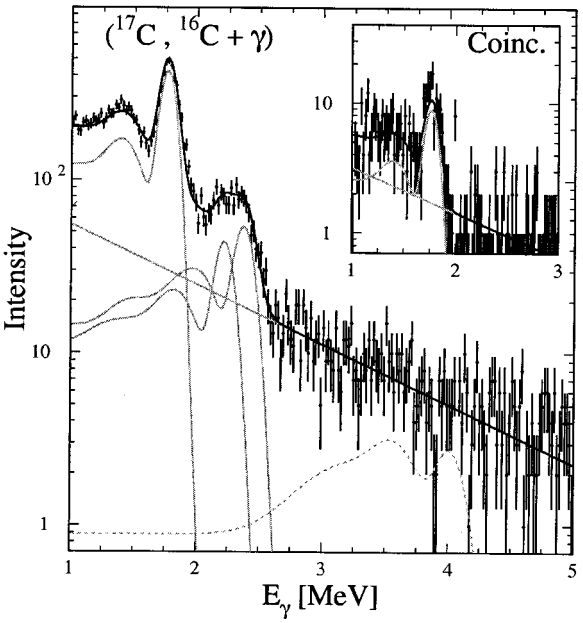

FIG. 4. Doppler-corrected γ-ray spectrum measured in ^{9}Be(^{17}C,^{16}C+γ)X. The black curve is a fit to the spectrum using an exponential curve for the background and response functions (grey curves) for each of the γ-ray transitions shown in the simplified level scheme of Fig. 5. The dashed line corresponds to an estimated upper limit of 2% for the direct transition from the $J=2$ level at 3.99 MeV to the ground state. Inset: γ spectrum gated on the transitions between the levels at $\simeq$4 MeV and the 2^+ level at 1.77 MeV. The spectrum was fitted using the same procedure described above.

The $\frac{3}{2}^+$ seniority-three neutron configuration appears at 0.096 MeV in ^{19}O. The USD spectroscopic factor for pickup from this $\frac{3}{2}^+$ state to the ground state of ^{18}O is $C^2S(0d_{3/2})=0.013$. This state is indeed populated very weakly in the ^{18}O(d,p)^{19}O reaction [79] and the observed angular distribution is characteristic of a multistep process. With the WBP interaction, the largest components of the ^{17}C $\frac{3}{2}^+$ state are 32% for $[(0p_{3/2})^8,(0p_{1/2})^2,(0d_{5/2})^3]$ and 31% for $[(0p_{3/2})^8,(0p_{1/2})^2,(0d_{5/2})^2,(1s_{1/2})^1]$, with the remaining 37% in small components. As in the ^{21}Ne and ^{19}O examples above, the $0d_{3/2}$ component is small resulting in $C^2S(0d_{3/2})=0.035$ for the ^{17}C $\frac{3}{2}^+$ state to the ^{16}C 0^+ ground state. As discussed in the next section, the strongest *sd* spectroscopic factors are to the excited 2^+ state in ^{16}C. The consequences and interpretation of this unusual situation will be discussed.

3. Experimental results

The Doppler-corrected γ-ray spectrum from the decay of the ^{16}C residues produced in one-neutron knockout reactions from ^{17}C is shown in Fig. 4. The simplified level scheme of ^{16}C, based on [61,62], is sketched in Fig. 5. The gamma peak

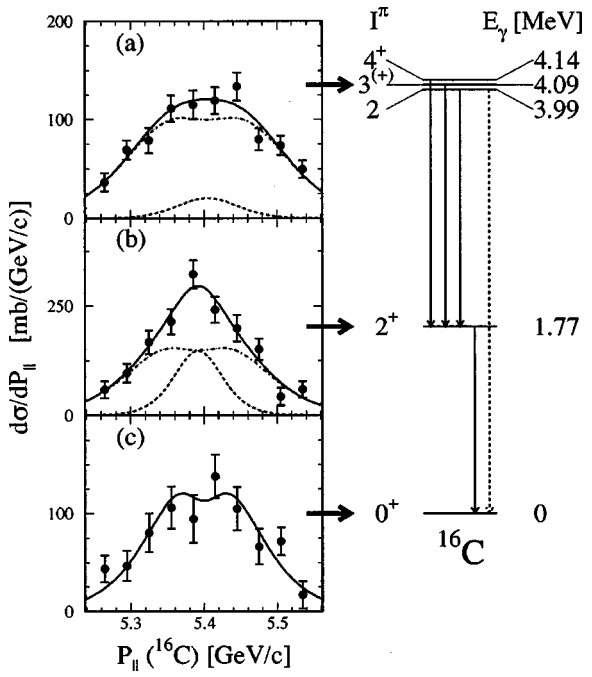

FIG. 5. Partial longitudinal momentum distributions corresponding to the states indicated in the simplified level scheme of ^{16}C. (a) and (b) The solid curves are the calculated momentum distributions with a mixture of *s* and *d* waves shown as dashed and dotted-dashed lines, respectively [8% *s* and 92% *d* in (a), 26% *s* and 74% *d* in (b)]. (c) The solid curve is the calculated momentum distribution of a pure *d* wave.

at 1.77 MeV arises in the decay from the first 2^+ level at 1.77 MeV to the ^{16}C ground state. The broad peak near 2.3 MeV is assumed to represent decays from the three (unresolved) levels near 4.1 MeV to the 2^+(1.77 MeV) state. The background was parametrized as an exponential, as in Fig. 2 and Refs. [6,8]. The total experimental spectrum was fitted with the individual response functions obtained from the Monte Carlo simulations superimposed on the background. This leads to the branching ratios $b_{\rm exp}$ given in Table I. The branch to the ground state of $19\pm9\%$ was obtained from an intensity balance; since this relatively large cross section disagrees with the shell-model calculations, we have examined whether the number would be consistent with zero. From the following analysis we conclude that there is definitely a substantial branch to this state.

An alternative explanation for the relatively strong cross section to the ground state would be the presence of unobserved γ rays, which would distort the intensity balance. Two possibilities were examined. The first would be a small direct branch to the ground state from the $J=2$ level near 4 MeV. An upper limit of 2% was estimated as shown by the dashed curve in Fig. 4. This is consistent with shell-model calculations. Another possibility would be that part of the intensity in the broad peak near 2.3 MeV would arise from a state of this energy decaying directly to the ground state. (No such state is known or expected [62].) Such a γ ray clearly would not be in coincidence with the 1.77γ ray, while the other 2.3 MeV γ rays are followed by this to 100%. We have examined this possibility by searching for triple coincidences (residue$-\gamma$-γ) in the data. With a gate on $E_\gamma \simeq 2.3$ MeV the spectrum, shown as an inset in Fig. 4, was obtained and fitted with the response function for the 1.77 MeV γ ray and an exponential background. The result was then compared on a quantitative basis with an event-by-event simulation generated with a γ ray from the first excited level at 1.77 MeV produced simultaneously with a γ ray from one of the three levels at $E\simeq 4.1$ MeV. The ratio between the experimental intensity for the coincident events and the intensity obtained in the simulation was $105\pm15\%$. The error limit would allow for at most a 5% (absolute) feeding of the ground state via such a mechanism, rather unlikely in the first place. These results support the level scheme assumed in the right-hand side of Fig. 5 and the branching ratios for the knockout cross section given in Tables I and II.

Yet another experimental effect that, at least in principle, might call the normalization into question and explain the enhanced cross section to the ^{16}C ground state would be the presence of the spin-parity $\frac{1}{2}^+$ state of ^{17}C as a contaminant isomer in the beam. This state has a reaction cross section that goes predominantly to the ground state of the residue; see Table II. We saw in connection with the analysis of the ^{16}C experiment in Sec. IV A 3 that a half-life of a few ns gave a mean flight path for the residues of 0.34 m. A half-life that was a factor 100 or more longer would allow isomers produced in the primary production target of the A1200 fragment separator to reach the experiment. Since the position of the $\frac{1}{2}^+$ state is unknown but presumably low in energy, such a long half-life is entirely possible. However, as will be discussed below, the momentum distribution belonging to this component would have a very characteristic $l=0$ shape in contradiction with the experiment, which gives $l=2$, as shown in Fig. 5. Hence also this explanation can be excluded.

The inclusive longitudinal momentum distribution of the ^{16}C residues was measured and found to be consistent with earlier measurements [11,15]. The estimated angular acceptance correction was 3.6%. From the γ coincidence information, the distribution could be separated into three components corresponding to feeding of the ground state, the 2^+ level, and the 4.1 MeV group of levels. In view of the relatively large error on the intensity of the ground-state branch, obtained by subtracting an 81% correction from the inclusive spectrum, we have verified that the shape remains stable within the error limits given. The reason for this is that the shapes for the excited levels are very similar, all three being dominated by $l=2$ components. The distributions were fitted with theoretical momentum distributions as described in Sec. III B assuming $l=0,2$ components, in the momentum range corresponding to the $\pm2.5\%$ instrumental momentum acceptance. The most interesting result was found for the distributions to the excited states, which are an admixture of *s* and *d* waves, with a dominant *d*-wave character in both cases ($92\pm8\%$ for the 4.1 MeV group of levels, and $74\pm10\%$ for the 2^+ state). This is the second case of a cross section with mixed l values observed in our experiments. [The reaction ^{9}Be(^{14}B,^{13}B$_{gs}$)X was found [7] to be predominantly $l=0$ with an $11\pm3\%$ $l=2$ admixture.] Finally, the cross section to the ^{16}C ground state is essentially $l=2$. The total inclusive

cross section, after extrapolation of momentum acceptance losses (estimated to be 2.4%), is 115 ± 14 mb, about two standard deviations above the value of 84 ± 9 mb measured [24] at 49 MeV/nucleon. The information supplied by the momentum distributions has made it possible to subdivide the measured cross section to the 1.77 MeV level into the l components given in Tables I and II. We now compare this evidence with the theoretical calculations.

The literature leaves two options for the ^{17}C spin, $\frac{1}{2}^+$ and $\frac{3}{2}^+$, as summarized in the preceding subsection. The absence of an $l=0$ reaction to the ^{16}C ground state is basically enough to fix the spin as $\frac{3}{2}^+$. This is actually the assignment that we propose and the one used in the discussion of the structure and spectroscopic factors in Table I. However, to demonstrate that the spectroscopic factors measured in the present work allow on their own a unique determination of the spin, we show in Table II the predicted cross sections and branching ratios for assumed spin-parity assignments of $\frac{1}{2}^+$ and $\frac{5}{2}^+$. The former is clearly excluded by the predicted dominance of *s*-wave knockout to the ground state with only weak branches to the excited states, both contradicted by experiment. Calculations for the case $J^\pi=\frac{5}{2}^+$, also listed in Table II, are also in disagreement with experiment, which has the main cross section to the 1.77 MeV 2^+ level and smaller branches to 0 and $\approx$4.1 MeV. The pattern predicted for an initial spin parity of $\frac{5}{2}^+$ is exactly opposite. Only the $J^\pi=\frac{3}{2}^+$ assignment for ^{17}C explains that the main part of the cross section goes to the 1.77 MeV 2^+ and about half as much to the 4.1 MeV group. Contrary to the statement made in Ref. [24], an $l=2$ momentum distribution and the inclusive cross section are insufficient for determining the ground-state spin and parity of ^{17}C as $J^\pi=\frac{3}{2}^+$. The only remaining difficulty is that the cross section to the ground state of ^{16}C of 22 mb is roughly one order of magnitude larger than expected. It has been argued above that this does not appear to be an experimental problem.

It is probably useful at this point to sum up in simple language some of the structural information conveyed by the ^{17}C results in Table I. We may think of the $\frac{3}{2}^+$ ground state as having three components, of which the main one is $0d_{5/2}\otimes[0d^2_{5/2}]_{2^+}$. This accounts for the dominant $l=2$ knockout to the 2^+ state. The smaller $l=0$ component to the same state arises from a small admixture of $1s_{1/2}\otimes[0d^2_{5/2}]_{2^+}$. There is excellent agreement between experiment and theory for both components. The predicted small cross section to the ^{16}C ground state comes from a small amount of $0d_{3/2}\otimes[0d^2_{5/2}]_{0^+}$ in the ^{17}C ground state and a simple explanation for the experimental result would be that theory for some reason underestimates this component. There are, however, other possibilities.

Our theory for calculating the cross sections, outlined in Sec. III B, assumes explicitly that the only reaction mechanism is the direct removal of a bound nucleon from a core of nucleons, which is otherwise a spectator. It is, however, possible to have contributions from other (higher order) mechanisms, such as the collective contributions, of order 10 mb, invoked to account for part of the (^{11}Be,^{10}Be) cross sections in Ref. [6]. Another possibility, recently investigated by Al-Khalili [80] is to allow the nucleon-target interaction to induce transitions between different single-particle states or between different m components of the same state. This mechanism, for the main $0d_{5/2}\otimes[0d^2_{5/2}]_{2^+}$ component discussed here, requires a spin-flip 0^+ recoupling of the two unstripped neutrons, and is estimated to contribute less than 1 mb.

C. The projectile ^{19}C

1. Previous experimental and theoretical work

The isotope ^{19}C occupies a position in the nuclear chart similar to that of ^{11}Be, and it has attracted much interest as a possible second candidate for a well-developed one-neutron halo state. This was suggested by the low adjusted value [71] of its one-neutron separation energy, $S_n=0.16\pm0.11$ MeV. This number represents the weighted average of measurements carried out at Los Alamos and GANIL [81,82]. The value of 0.24 MeV often encountered in the literature includes, in addition, two earlier and less precise measurements by the same groups in the weighted average.The adjustment [71] normally excludes such results from its recommendation. Indirect evidence discussed below suggests that a value larger than 0.16 MeV, i.e., 0.5–1.0 MeV, is required to interpret the data in a consistent way.

Several previous experiments have investigated the structure of ^{19}C by measuring the longitudinal momentum distributions of the core fragments ^{18}C [11,15]. The narrow widths observed in these experiments resemble those found for ^{11}Be and were suggestive of a halo structure. They were, however, wider than the adjusted neutron separation energy value would allow, which prompted speculations that the ^{19}C ground state is dominated by complex-structure components. Bazin *et al.* [11], however, pointed out that the momentum distribution in the Coulomb breakup of ^{19}C could be understood if the neutron separation energy was about 0.6 MeV. An experiment by Marqués *et al.* [12] observed neutrons from ^{19}C breakup reactions in which neutrons were detected in coincidence with charged fragments with charge five and lower. They found a broad component in the angular distribution, which they associated with nucleus-nucleus collisions. A narrow component with a Lorentzian width parameter Γ of 55 MeV/c was taken as evidence for a halo neutron present as a spectator in the collision.

A recent experiment on the Coulomb dissociation of ^{19}C on a lead target by Nakamura *et al.* [18] represents a decisive step forward. They found that the angular distribution of the decaying ^{18}C$+n$ system required a neutron separation energy S_n of 0.53 ± 0.13 MeV and also that with this energy they could understand the differential cross section as a function of the relative energy of the dissociation products, which was not the case for a value of 0.16 MeV. The absolute Coulomb cross section (neglecting possible contributions to excited levels, discussed below) leads to a spectroscopic factor of 0.67, thus showing that the dominant character of the ^{19}C ground state is $1s_{1/2}\otimes0^+$. Since this analysis does not correct for branches to excited states, which are expected to be present, also for the Coulomb part of the cross section, the results should be taken as qualitative.

Interaction cross section measurements have also been reported for ^{19}C on ^{12}C at 960 MeV/nucleon [17]. The analysis of these data in a few-body Glauber theory approach has shown [20] that the measured σ_I are consistent with a $J^\pi = \frac{1}{2}^+$ ^{19}C ground state, while excluding $J^\pi = \frac{3}{2}^+$ and $J^\pi = \frac{5}{2}^+$ assignments. In particular, the σ_I datum was found to be consistent with a dominant $1s_{1/2} \otimes 0^+$ configuration for separation energy values ranging between 0.12 and 0.65 MeV, with spectroscopic factors between 0.7 and 1.0. This result is consistent with the separation energy value found from the Coulomb dissociation experiment [18] and with the results reported below.

A number of papers have discussed the structure and reactions of ^{19}C, primarily in the light of particle-core coupling models [13,14,16,19,56,22,23,25]. We mention in passing an attempt by Smedberg and Zhukov [19] to account for a perceived difference in longitudinal momentum widths observed at 77 MeV/nucleon [11] and at 910 MeV/nucleon [15]. They invoked an additional reaction mechanism involving an unspecified intermediate resonance just above the $^{18}C+n$ threshold. This hypothesis does not find support in the present work, where we analyze 62 and 910 MeV/nucleon data in more detail below. In another analysis, Kanungo *et al.* [25] found it difficult to reconcile the ^{19}C momentum distributions at the two energies with the measured interaction cross section. As a remedy they proposed that the core of ^{19}C is considerably larger than that of free ^{18}C.

2. Present shell-model results

In the following we compare with shell-model calculations [40], which predict the presence of three bound states above the ground state of ^{18}C. There are two 2^+ levels at 2.1 MeV (observed experimentally at 1.62 ± 0.02 [73]) and at 3.4 MeV. A 0^+ level at 4.0 MeV, just below the neutron threshold of 4.2 MeV, is expected to decay by a cascade of 1.6 and 2.4 MeV γ rays, and it has a large $l=0$ spectroscopic factor that would contribute noticeably to the Coulomb cross section. There are two more states (2^+, 3^+) close in energy, near 4.9 MeV, which we include in the analysis, observing that the calculations tend to overestimate the level energies by several hundreds of keV. The lowest levels in ^{19}C are predicted to be ($\frac{5}{2}^+$,0.00), ($\frac{1}{2}^+$,0.05), ($\frac{3}{2}^+$,0.40) with energies in MeV. We take the spin-parity assignment for the ground state to be established by the Coulomb dissociation experiment [18]. It will be seen below that the same conclusion can be reached independently from our data. With the WBP parameters [40] we obtain the spectroscopic factors given in Table I, where we leave out the 3.4 MeV level for which the spectroscopic factors are small (total 0.10 for $l=2$).

As discussed in Sec. III A, the WBP and WBT interactions both present a triplet of low-lying states for ^{19}C. The present experimental results are in agreement only with the spectroscopic factors based upon the $\frac{1}{2}^+$ ground state. The WBP interaction gives a $\frac{1}{2}^+$ ground state and this will be used for further comparisons. However, for the given spin-parity of $\frac{1}{2}^+$, the spectroscopic factors are very similar between WBP and WBT.

With WBP the largest component of the ^{19}C $\frac{1}{2}^+$ state is 48% for $[(0p_{3/2})^8,(0p_{1/2})^2,(0d_{5/2})^4,(1s_{1/2})^1]$ with the remaining 52% in smaller components. The $[(0d_{5/2})^4,(1s_{1/2})^1]$ configuration appears at an excitation energy of 1.33 MeV in ^{21}O with the USD interaction [40], and may be associated with an experimental state observed at the same energy [75]. In the framework of WBP (and WBT) its energy is lowered in ^{19}C due to the 1.6 MeV downward shift of the $1s_{1/2}$ state relative to $0d_{5/2}$ between ^{17}O and ^{15}C.

3. Experimental results

In spite of the low intensity of the incident ^{19}C ($\simeq$0.5–1 particles/s), enough information was collected in different reaction channels to confirm that its ground state is a well-developed halo state. We discuss this evidence in the following, first the γ-coincidence information leading to the ground state partial cross section and exclusive momentum distribution, second the inclusive momentum spectrum, and, third, the exclusive cross section for Coulomb dissociation to the ^{18}C ground state. We demonstrate that the evidence combines to give a consistent set of parameters for the halo state.

The γ-ray spectrum in coincidence with projectile residues had too little statistics for it to be analyzed with the peak-fitting procedure used in the case of ^{17}C. Instead we used all gamma rays above 0.25 MeV as a tag identifying γ-coincident events and applied a correction based on the average gamma efficiency to the residual noncoincident events. (This was the experimental approach taken previously in our work on the phosphorus isotopes [4].) The branching ratio listed in Table I and the ground-state momentum distribution shown in Fig. 6 were then obtained as follows.

The gamma spectra from (^{16}C,^{15}C) and (^{12}Be,^{11}Be), which have no γ rays above 0.74 and 0.32 MeV, respectively, and also the previous analysis of the (^{11}Be,^{10}Be) reaction [6] indicate the presence of a structureless continuum distribution that depends approximately exponentially on the energy. With an integral cutoff at 0.25 MeV, the intensity of this per fragment is approximately 9% for the three cases, and the corresponding coincident momentum distribution is very similar to that of the inclusive spectrum. The average detection efficiency for the excited levels was calculated in the GEANT Monte Carlo simulations and gave for the 1.6 and 2.4 γ rays the efficiencies $\epsilon_1 = 23\%$ and $\epsilon_2 = 22.6\%$, respectively. Assuming that the states near 4 MeV decay through the 1.6 MeV state, the cascade detection efficiency is around 41%. The total efficiency was then estimated to be 38%, using the relative intensities predicted by theory. With these values, the resulting branching ratio to the ground state was $56 \pm 9\%$, consistent within the error with the result that would be obtained if the theoretically predicted levels near 4 MeV were not populated, i.e., if they were above the neutron threshold. The branching ratio has been corrected for the momentum acceptance of the spectrometer, which eliminates the ''tails'' of the momentum distributions, especially for the $l=2$ component. The corrections are based on the theoretical momentum distributions for a neutron separation energy of 0.8 MeV and assumed the theoretical branching ratios of the excited states. This leads to the partial cross section of

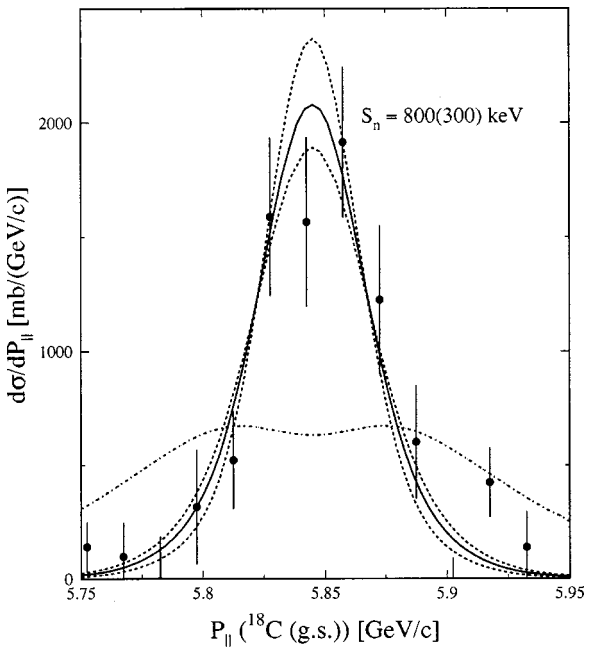

FIG. 6. Longitudinal momentum distribution corresponding to the ground state of the ^{18}C residues after one-neutron removal from ^{19}C on a ^{9}Be target. The coincidences with γ rays have been used to correct the inclusive distribution for contributions from excited levels. The momentum distribution corresponding to the extracted separation energy $S_n = 0.8$ MeV is represented by the solid line. The dashed lines represent the momentum distributions corresponding to separation energies of 0.5 and 1.1 MeV. The dotted-dashed curve is calculated for a d state for a separation energy of 0.8 MeV.

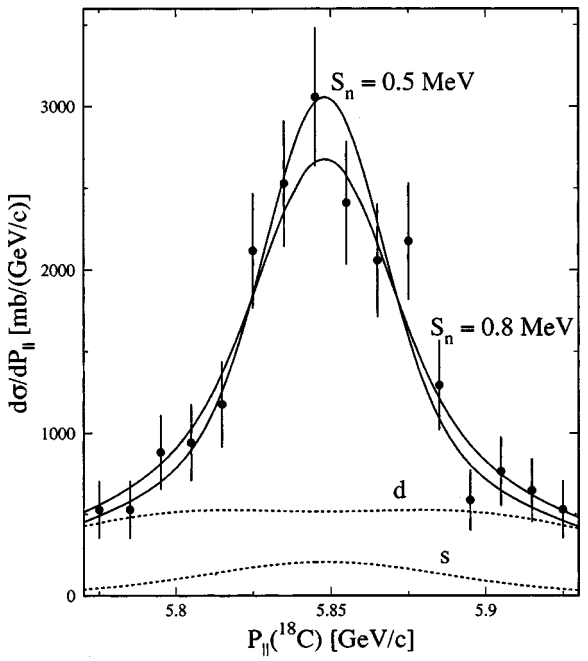

FIG. 7. Inclusive longitudinal momentum distribution corresponding to ^{18}C residues after one-neutron removal from ^{19}C on a ^{9}Be target. The solid lines represent the calculated inclusive momentum distributions corresponding to $S_n = 0.5$ and $S_n = 0.8$ MeV obtained as a least-squares fit assuming the branching ratios given by the theoretical spectroscopic factors of Table I. These values represent approximately the $\pm 1\sigma$ limits of the allowed interval and correspond to a χ^2 of 8 and 9, respectively, for 14 degrees of freedom. (For $S_n = 0.3$ and $S_n = 1.1$ MeV χ^2 increases to 18 and 14, respectively.) The dashed lines labeled with s and d represent the contributions from the $l = 0,2$ excited states for $S_n = 0.8$ MeV. Their contributions for $S_n = 0.5$ MeV would be almost identical.

148 ± 50 mb, a large value typical of a halo state.

The analysis based on integral-bias gamma tagging also leads to the ground-state momentum distribution shown in Fig. 6, narrow and consistent with an s-state halo structure. The calculations are based on the black-disk model discussed above. Together with the large partial cross section this proves the ground-state spin-parity of ^{19}C to be $J^\pi = \frac{1}{2}^+$, in agreement with the analyses of [18,17,20]. The width of the momentum distribution is quite sensitive to the separation energy; a least-squares adjustment suggests a value $S_n = 0.8 \pm 0.3$ MeV.

An alternative way of testing the dependence on the assumed value of S_n is to fit the inclusive momentum distribution, i.e., without the gamma coincidence requirement, of the ^{18}C residues. For this analysis we assume the theoretical spectroscopic factors given in Table I. The adjusted momentum distributions for the assumed values $S_n = 0.5$ and 0.8 MeV are shown in Fig. 7. The result of the least-squares analysis was $S_n = 0.65 \pm 0.15$ MeV, which gives a branching ratio to the ground state of $48 \pm 2\%$ in good agreement with the $56 \pm 9\%$ obtained in the gamma coincidence analysis. This result is in quantitative agreement with the coincidence analysis of the ground state momentum distribution.

Another inclusive spectrum of the projectile residues has been obtained for ^{19}C on a ^{12}C target at 910 MeV/nucleon in a GSI experiment [15]. This distribution is close to identical to that of Fig. 7, and both are marginally consistent with that given by [11], which has much poorer statistics. For this result, adjustment of a theoretical momentum distribution similar to that in Fig. 7 leads to a somewhat lower branch to the ground state, 40% as compared with the 48% found at our energy in the same analysis. The smaller value is to a large extent accounted for by smaller nucleon-nucleon cross sections and real-to-imaginary amplitudes at the higher energy. An analysis for 910 MeV/nucleon on a carbon target and with the theoretical spectroscopic factors of Table I reduces the theoretical ground-state branch to 40% from the 46% obtained for a beryllium target at 57 MeV/nucleon. We conclude that the experiment of Baumann *et al.* [15], is entirely consistent with ours.

Finally, data that we had taken for reactions of ^{19}C on a Au target were also used to provide a constraint on the parameters. We found an inclusive (^{19}C, ^{18}C) cross section on the gold target of 1.35 ± 0.18 b at 56 MeV/nucleon, which is close to the value of 1.34 ± 0.12 b observed in the (^{19}C, ^{18}C $+ n$) channel on a lead target at 67 MeV/nucleon [18]. In order to compare more precisely, we add an (unobserved) absorptive part assumed to be 0.15 b to the cross section of Nakamura *et al.* [18] (their estimate) and we scale their Coulomb part of the cross section with the inverse of the beam energy and with the square of the target charge number. This yields an equivalent cross section of 1.53 ± 0.14 b under our conditions in excellent agreement with our value of 1.35

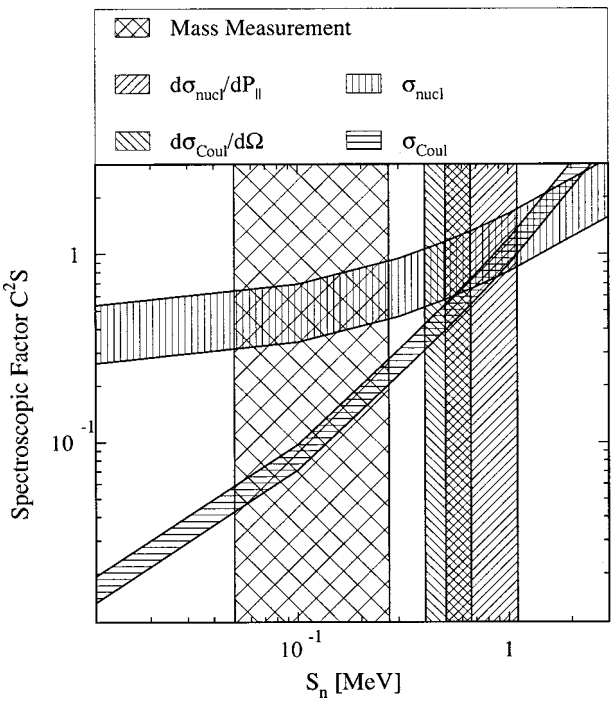

FIG. 8. Permitted regions in the space of spectroscopic factor and one-neutron separation energy for the ground state of ^{19}C. The hatched areas result from different information: measured nuclear and Coulomb breakup cross sections (σ_{nucl}, σ_{Coul}) and momentum distribution analysis ($d\sigma/dP_{||}$). Also shown are the result from the Coulomb dissociation experiment in Ref. [18], deduced from $d\sigma/d\Omega$, and the separation energy value in Ref. [71]. A consistent description of the experimental results is given for values of C^2S between 0.5 and 1 and of S_n between 0.5 and 1 MeV. Note that this graph does not display the two analyses of inclusive momentum distributions discussed in the text.

± 0.18 b. Since our experiment observed gamma rays in coincidence with the projectile residue, we could use the gamma-ray tagging method described above for finding that $85\pm 7\%$ of the total cross section connects to the ground state corresponding to an absolute value of 1.15 ± 0.18 b. The contribution from the continuum distribution is considerably higher from a gold target than from a beryllium target, especially at low energies. For this reason we increased the bias setting for the tag to 1 MeV. The yield from the continuum part of the spectrum was then 12% as could be deduced from the Au(^{16}C,^{15}C)X data (it would have been 4% with a Be target) and the detection efficiency was estimated (in the same fashion as for the beryllium target) to be $\epsilon_{\mathrm{tot}}=24.3\%$. The deduced ground-state cross section could now be compared with theoretically calculated single-particle cross sections based on the assumption that nuclear and Coulomb contributions are additive. The nuclear part was calculated as in Ref. [5] and the electromagnetic part as in Ref. [83].

It will be clear that the neutron separation energy and the ground-state spectroscopic factor both must be considered unknown parameters. We use the data discussed above to place constraints in the S_n-C^2S plane as shown in Fig. 8, where the boundaries corresponding to the five sets of input data indicate limits corresponding to plus or minus one standard deviation. Two cross-hatched areas represent limits on S_n. One is from the analysis of the momentum width shown in Fig. 6 and the other from the differential cross section $d\sigma/d\Omega$ as a function of the center-of-mass deflection angle [18]. Two other regions of the S_n-C^2S plane, marked with vertical and horizontal lines, denote limits obtained from the absolute partial cross sections on beryllium and gold, respectively. The Coulomb cross section is based on our value; the result of Nakamura *et al.* would place the curve slightly higher but still within the error band. Four of the allowed bands point to a single consistent solution corresponding to a neutron separation energy of 0.5–1.0 MeV and a spectroscopic factor of 0.5–1.0 (theoretical value 0.58). This allows the conclusion that the ground state of ^{19}C has a well developed halo, similar to that of ^{11}Be. The fifth band, representing the direct mass measurement, does not allow a solution consistent with the other experimental input.

Since the lack of precise knowledge of the ^{19}C mass has been a main obstacle to our understanding of this case, it should be clear that it would be extremely valuable to have an accurate direct measurement. Still, it is probably useful at this point to summarize the indirect evidence. The analysis based on integral gamma tagging (Fig. 6) is free from evident systematic errors, but suffers from low statistics. This leads to the rather imprecise value of the neutron separation energy, $S_n=0.8\pm 0.3$ MeV, which, nevertheless, has been used for the analysis of the cross sections in Table I. The values obtained from the analysis of the inclusive momentum spectrum (Fig. 7), 0.65 ± 0.15 MeV, and from the Coulomb dissociation experiment by Nakamura *et al.* [18], 0.53 ± 0.13 MeV, are both more appealing. They suffer, however, from uncertainties concerning the contributions from excited levels, which were taken from theory in the former case and neglected in the latter. The absolute nuclear and electric cross sections of Fig. 8 are again consistent with the three values given here, and all approaches give definitely larger values for the separation energy than the 0.16 ± 0.11 MeV based on the direct mass measurements. It would probably be premature to propose a combined value at this moment.

V. CONCLUDING REMARKS

In this and previous papers we have demonstrated that knockout reactions offer a very promising spectroscopic tool that can test nuclear structure theory in considerable detail. This technique also has the high sensitivity that is a prerequisite for experiments with beams of rare isotopes. Our best example of this, so far, is Fig. 8, for which the main part of the data was obtained in reactions induced by an incident (secondary) beam of ^{19}C of slightly less than one atom per second. (The results for ^{25}F recently presented by Sauvan *et al.* [24] used a similar beam intensity.) This information has been sufficient for determining the spin and parity of the ground state and for showing that it is a neutron halo state with a spectroscopic factor approaching unity. This is the second established case of a pronounced single-neutron halo beyond ^{11}Be, although ^{14}B and ^{15}C might also be considered as qualifying for this epithet. All the measurements reported here have been limited by counting statistics and by the me-

diocre resolution of the NaI(Tl) gamma detectors. Very soon better measurements, based on a more powerful radioactive-beam facility and on segmented germanium detectors, should become possible.

Theory is the second essential ingredient in the kind of studies presented here. One cannot overestimate the importance of basing experiments and analysis on rigorous theoretical models with a predetermined set of parameters and, if possible, offering a clear choice of alternatives. In the field of exotic nuclei, where out of necessity only a limited amount of experimental information is available, there is clearly a danger in working from flexible models that can be tailored to the needs of each individual nucleus and that, seen in isolation, may seem plausible. We have used a version of the many-particle shell-model that accounts very well for both single-particle and collective variables, and we demonstrate in Table I how a combination of l assignments and spectroscopic factors can provide very detailed tests of nuclear structure. In the case of ^{17}C we can firmly retain a $\frac{3}{2}^+$ spin-parity assignment, cf. the predictions for the excluded alternatives given in Table II. Note also that the experiment successfully confirms the predicted 20% admixture of $l=0$ in the predominantly $l=2$ knockout to the 2^+ level. An interesting open theoretical problem is how the knockout reactions should be applied to nuclei with strong permanent quadrupole deformations. Recently, Sakharuk and Zelevinsky [84] performed a first investigation of this problem with a simplified theory and applied the results to the reaction (^{25}Na,^{24}Mg). The effects are very pronounced, especially for Nilsson states with low values of the projection quantum number Ω. The momentum distributions to members of the ^{24}Mg ground-state rotational band vary in shape and intensity with spin and suggest a rich source of information that calls to mind the ''fingerprints'' seen in transfer reactions at low energy on rare-earth nuclei [1].

The absolute precision of the method still is an open question. We have, until now, investigated l values and spectroscopic factors in about 20 partial cross sections for proton and neutron removal reactions in the p and sd shells, and seem to find consistent results. In a previous paper [8], we have offered preliminary estimates of the experimental and theoretical errors and arrive in both ways at a relative value of $\pm 20\%$. It remains to be seen whether this holds (or improves) as more evidence accumulates, or whether there will be a need for fine-tuning the theory. Our current impression is that the knockout reactions show promise of becoming an interesting precision complement to the classical pickup reactions at low beam energies.

A more fundamental question is why there is such good agreement between experimental and theoretical cross sections. The connection between the two is provided by Eq. (1), which supplies the heuristic link between two seemingly unconnected theories. The spectroscopic factors are defined in a severely truncated Hilbert space with nucleons assumed to be the fundamental building blocks. These are subject to effective interactions, which take values adjusted to compensate for the neglected degrees of freedom. The reaction theory used for calculating the stripping and diffraction dissociation cross sections also, as it seems successfully, starts from a picture of quasi-free nucleons, generally believed to be valid at very high energies. Essential input parameters are nucleon densities and free nucleon–nucleon scattering cross sections. In the present work, this version of Glauber theory is applied well below the energy at which it is usually assumed to become a good approximation. In both calculations we have relied on pre-existing parameter selections and have obtained good agreement on an absolute scale.

It is tempting to speculate that this agreement is not a mere coincidence. The reason could be that the reactions are surface dominated [5,53], and that they sample predominantly the nuclear exterior. In this region, where the density is low, we may expect the nucleons of the effective-interaction theory to have properties close to those of a free nucleon. To give a rough quantitative scale for the average size of the exterior sampled in the experiments, consider, for the case of a beryllium target, the ratio of a typical single-particle stripping cross section of about 30 mb to the free-neutron reaction cross section at the same energy of 300 mb. This means that the observed cross sections represent the outer 10% of the single-particle wave function. The same argument is the key point in the analysis of the momentum distributions [35–37], namely that the reactions sample just the momentum content of this external region and are blind to contributions from the (unexplored) interior. As was alluded to in the Introduction to the present paper, the dominance of the nuclear surface is a general characteristic of nuclear spectroscopy via transfer reactions at lower energies. The same effect appears in a slightly different disguise in experiments designed to draw inferences about reactions of astrophysical interest by measuring asymptotic normalization coefficients of single-particle wave functions at large distances, as in [85] and other work cited therein. In contrast to this, experiments with electrons and other purely electromagnetic probes can give information relating to the nuclear interior. Dieperink and de Witt Huberts [86] find that the general occupancy of single-particle proton orbitals below the Fermi surface, as determined from the charge densities, is only $75\pm 10\%$ rather than unity and that for $(e,e'p)$ single-proton removal reactions, the reduction can be even more drastic. For the nucleus most relevant to those discussed in the present paper, ^{12}C, the spectroscopic factors to the $\frac{3}{2}^-$ and $\frac{1}{2}^-$ states of ^{11}B are only 65% and 50%, respectively, of the values predicted by a shell-model calculation similar to the one used here. One may speculate that these differences are connected with nuclear-matter effects that are not directly relevant to nuclear shell structure. In this connection it is suggestive that the experimental charge density for the $4s_{1/2}$ proton in the outer 5–8 fm of ^{208}Pb seems to be above or close to the theoretical single-particle density while it is below elsewhere [87]. The question as to what precisely are the quantities determined in our experiments and why the approach works so well is clearly one that deserves further study.

The experiment involving the excited level of ^{15}C showed that isomeric states produced in the knockout reaction can give rise to experimental complications and serves as a reminder that it may be prudent (as well as rewarding) in gen-

eral to carry out a separate search for possible unknown isomers in the outgoing residues (what one could call the ''tertiary beam''). The presence of isomers in the secondary beam from fragmentation has already allowed Grzywacz *et al.* [88] to discover a number of interesting new isomers. This suggests as another possibility the use of the techniques discussed in the present paper for investigating spectroscopic reactions of isomers. If the outcome of the reactions were sufficiently different, the presence of two species in the beam may not be an unsurmountable obstacle, provided that the ratio of the intensities were known from direct experiments.

ACKNOWLEDGMENTS

This work was supported by NSF Grant Nos. PHY 9528844 and PHY 0070911. The support of EPSRC (U.K.) Grant No. GR/M82141, for J.A.T., is also acknowledged. We would like to thank D. John Millener for many interesting discussions.

[1] Aa. Bohr and B.R. Mottelson, *Nuclear Structure* (Benjamin, New York, 1969), Vol. 1, p. 420; *ibid.* Vol. 2, pp. 243 and 258.
[2] G.R. Satchler, *Direct Nuclear Reactions* (University Press, Oxford, 1983).
[3] H. Feshbach, *Theoretical Nuclear Physics: Nuclear Reactions* (Wiley, New York, 1992), p. 455.
[4] A. Navin *et al.*, Phys. Rev. Lett. **81**, 5089 (1998).
[5] J.A. Tostevin, J. Phys. G **25**, 735 (1999).
[6] T. Aumann *et al.*, Phys. Rev. Lett. **84**, 35 (2000).
[7] V. Guimarães *et al.*, Phys. Rev. C **61**, 064609 (2000).
[8] A. Navin *et al.*, Phys. Rev. Lett. **85**, 266 (2000).
[9] L. Chen, B. Blank, B.A. Brown, M. Chartier, A. Galonsky, P.G. Hansen, and M. Thoennessen (unpublished).
[10] K. Hencken, G. Bertsch, and H. Esbensen, Phys. Rev. C **54**, 3043 (1996).
[11] D. Bazin *et al.*, Phys. Rev. Lett. **74**, 3569 (1995); Phys. Rev. C **57**, 2156 (1998).
[12] F.M. Marqués *et al.*, Phys. Lett. B **381**, 407 (1996).
[13] D. Ridikas, M.H. Smedberg, J.S. Vaagen, and M.V. Zhukov, Europhys. Lett. **37**, 385 (1997).
[14] D. Ridikas, M.H. Smedberg, J.S. Vaagen, and M.V. Zhukov, Nucl. Phys. **A628**, 363 (1998).
[15] T. Baumann *et al.*, Phys. Lett. B **439**, 256 (1998).
[16] P. Banerjee, I.J. Thompson, and J.A. Tostevin, Phys. Rev. C **58**, 1042 (1998).
[17] A. Ozawa *et al.*, RIKEN Report No. RIKEN-AF-NP-294, 1998.
[18] T. Nakamura *et al.*, Phys. Rev. Lett. **83**, 1112 (1999).
[19] M.H. Smedberg and M.V. Zhukov, Phys. Rev. C **59**, 2048 (1999).
[20] J.A. Tostevin and J.S. Al-Khalili, Phys. Rev. C **59**, R5 (1999).
[21] L.V. Chulkov *et al.*, Nucl. Phys. **A674**, 330 (2000).
[22] R. Chatterjee, P. Banerjee, and R. Shyam, Nucl. Phys. **A675**, 477 (2000).
[23] P. Descouvemont, Nucl. Phys. **A675**, 559 (2000).
[24] E. Sauvan *et al.*, Phys. Lett. B **491**, 1 (2000).
[25] R. Kanungo, I. Tanihata, Y. Ogawa, H. Toki, and A. Ozawa, Nucl. Phys. **A677**, 171 (2000).
[26] B.M. Sherrill, D.J. Morrissey, J.A. Nolen, Jr., N. Orr, and J.A. Winger, Nucl. Instrum. Methods Phys. Res. B **70**, 298 (1992).
[27] H. Scheit, T. Glasmacher, R.W. Ibbotson, and P.G. Thirolf, Nucl. Instrum. Methods Phys. Res. A **422**, 124 (1999).
[28] B.M. Sherrill *et al.* (unpublished); J.A. Caggiano, Ph.D. thesis, Michigan State University, 1999.
[29] J. Yurkon, D. Bazin, W. Benenson, D.J. Morrissey, B.M. Sherrill, D. Swan, and R. Swanson, Nucl. Instrum. Methods Phys. Res. A **422**, 291 (1999).
[30] M. Berz, K. Joh, J.A. Nolen, B.M. Sherrill, and A.F. Zeller, Phys. Rev. C **47**, 537 (1993).
[31] GEANT, Cern Library Long Writeup W5013, 1994.
[32] P.G. Hansen, A.S. Jensen, and B. Jonson, Annu. Rev. Nucl. Part. Sci. **45**, 591 (1995).
[33] G. Bertsch, H. Esbensen, and A. Sustich, Phys. Rev. C **42**, 758 (1990).
[34] K. Yabana, Y. Ogawa, and Y. Suzuki, Nucl. Phys. **A539**, 293 (1992).
[35] P.G. Hansen, in *Proceedings of the International Conference on Exotic Nuclei and Atomic Masses, Arles, France, June 1995*, edited by M. de Saint Simon and O. Sorlin (Editions Frontières, Orsay, 1995), pp. 175–186.
[36] P.G. Hansen, Phys. Rev. Lett. **77**, 1016 (1996).
[37] H. Esbensen, Phys. Rev. C **53**, 2007 (1996).
[38] J.H. Kelley *et al.*, Phys. Rev. Lett. **74**, 30 (1995).
[39] M.S. Hussein and K.W. McVoy, Nucl. Phys. **A445**, 124 (1985).
[40] B.A. Brown and B.H. Wildenthal, Annu. Rev. Nucl. Part. Sci. **38**, 29 (1988); the USD energy levels are given at www.nscl.msu.edu/brown/sde.htm
[41] E.K. Warburton and B.A. Brown, Phys. Rev. C **46**, 923 (1992).
[42] D.J. Millener and D. Kurath, Nucl. Phys. **A255**, 315 (1975).
[43] B.A. Brown, in *ENAM95*, edited by M. de Saint Simon and O. Sorlin (Editions Frontières, Gif-sur-Yvette, 1995), p. 451; in *International School of Heavy-Ion Physics, 4th Course: Exotic Nuclei*, edited by R.A. Broglia and P.G. Hansen (World Scientific, Singapore, 1998), p. 1.
[44] J.S. Al-Khalili, J.A. Tostevin, and I.J. Thompson, Phys. Rev. C **54**, 1843 (1996).
[45] J.A. Tostevin and J.S. Al-Khalili, Nucl. Phys. **A616**, 418 (1997).
[46] R.J. Glauber, in *Lectures in Theoretical Physics*, edited by W.E. Brittin (Interscience, New York, 1959), Vol. 1, p. 315.
[47] S.K. Charagi and S.K. Gupta, Phys. Rev. C **41**, 1610 (1990).
[48] L. Ray, Phys. Rev. C **20**, 1857 (1979).
[49] S. Kox *et al.*, Phys. Rev. C **35**, 1678 (1987).
[50] P.U. Renberg, D.F. Measday, M. Pepin, P. Schwaller, B. Favier, and C. Richard-Serre, Nucl. Phys. **A183**, 81 (1972).
[51] M.G. Saint-Laurent *et al.*, Z. Phys. A **332**, 457 (1989).
[52] E. Liatard *et al.*, Europhys. Lett. **13**, 401 (1990).
[53] J.A. Tostevin, in *Fission and Properties of Neutron-rich Nuclei*, Proceedings of the Second International Conference, St.

Andrews, Scotland, 1999, edited by J.H. Hamilton, W.R. Phillips, and H.K. Carter (World Scientific, Singapore, 2000), p. 429.
[54] A. Bonaccorso and D.M. Brink, Phys. Rev. C **57**, R22 (1998).
[55] A. Bonaccorso and D.M. Brink, Phys. Rev. C **58**, 2864 (1998).
[56] A. Bonaccorso, Phys. Rev. C **60**, 054604 (1999).
[57] A. Bonaccorso (private communication).
[58] H.T. Fortune, R. Middleton, M.E. Cobern, G.E. Moore, S. Mordechai, R.V. Kollaritis, H. Nann, W. Chung, and B.H. Wildenthal, Phys. Lett. **70B**, 408 (1977).
[59] H.T. Fortune, M.E. Cobern, S. Mordechai, G.E. Moore, S. Lafrance, and R. Middleton, Phys. Rev. Lett. **40**, 1236 (1978).
[60] R.R. Sercely, R.J. Peterson, and E.R. Flynn, Phys. Rev. C **17**, 1919 (1978).
[61] D.P. Balamuth, J.M. Lind, K.C. Young, Jr., and R.W. Zurmühle, Nucl. Phys. **A290**, 65 (1977).
[62] D.R. Tilley, H.R. Weller, and C.M. Cheves, Nucl. Phys. **A564**, 1 (1993).
[63] R.D. Lawson, F.J.D. Serduke, and H.T. Fortune, Phys. Rev. C **14**, 1245 (1976).
[64] R. Sherr and H.T. Fortune, Phys. Rev. C **58**, 3292 (1998).
[65] H.T. Fortune, M.E. Cobern, S. Mordechai, G.E. Moore, S. Lafrance, and R. Middleton, Phys. Rev. Lett. **40**, 1236 (1978).
[66] M. Zahar *et al.*, Phys. Rev. C **48**, R1484 (1993).
[67] M.D. Belbot *et al.*, Phys. Rev. C **51**, 2372 (1995).
[68] U.C. Bergmann *et al.*, Nucl. Phys. **A658**, 129 (1999).
[69] N.K. Timofeyuk and P. Descouvemont, J. Phys. G **22**, L99 (1996).
[70] M. Labiche, F.M. Marqués, O. Sorlin, and N. Vinh Mau, Phys. Rev. C **60**, 027303 (1999).
[71] G. Audi and A.H. Wapstra, Nucl. Phys. **A565**, 1 (1993); G. Audi, O. Bersillon, J. Blachot, and A.H. Wapstra, *ibid.* **A624**, 1 (1997).
[72] F. Ajzenberg-Selove, Nucl. Phys. **A523**, 1 (1991).
[73] L.K. Fifield, J.L. Durell, M.A.C. Hotchkis, J.R. Leigh, T.R. Ophel, and D.C. Weisser, Nucl. Phys. **A385**, 505 (1982).
[74] E.K. Warburton and D.J. Millener, Phys. Rev. C **39**, 1120 (1989).
[75] W.N. Catford, L.K. Fifield, N.A. Orr, and C.L. Woods, Nucl. Phys. **A503**, 263 (1989).
[76] J.P. Dufour, R. del Moral, A. Fleury, F. Hubert, D. Jean, M.S. Pravikoff, H. Delagrange, H. Geissel, and K.H. Schmidt, Z. Phys. A **324**, 487 (1986).
[77] M.S. Curtin, L.H. Harwood, J.A. Nolen, B. Sherrill, Z.Q. Xiee, and B.A. Brown, Phys. Rev. Lett. **56**, 34 (1986).
[78] P.M. Endt, At. Data Nucl. Data Tables **19**, 23 (1977).
[79] J.L. Wiza and R. Middelton, Phys. Rev. **143**, 676 (1966).
[80] J. Al-Khalili (private communication).
[81] J. Wouters *et al.*, Z. Phys. A **331**, 229 (1988).
[82] N. Orr *et al.*, Phys. Lett. B **258**, 29 (1991).
[83] D.M. Kalassa and G. Baur, J. Phys. G **22**, 115 (1996).
[84] A. Sakharuk and V. Zelevinsky, Phys. Rev. C **61**, 014609 (1999).
[85] A.M. Mukhamedzhanov and R.G. Tribble, Phys. Rev. C **59**, 3418 (1999).
[86] A.E.L. Dieperink and P.K.A. de Witt Huberts, Annu. Rev. Nucl. Part. Sci. **40**, 239 (1990).
[87] P.K.A. de Witt Huberts, Nucl. Phys. **A649**, 3 (1999).
[88] R. Grzywacz *et al.*, Phys. Rev. Lett. **81**, 766 (1998); Phys. Lett. B **355**, 439 (1995); Phys. Rev. C **55**, 1126 (1997).